Technical note

To:	NVE
Attn.:	Odd-Arne Jensen
Copy to:	
Date:	2021-03-22
Revision no./Rev.date:	0 /
Document no.:	20200017-04-TN
Project:	AARN - Applied Avalanche Research in Norway
Project manager:	Christian Jaedicke
Prepared by:	Peter Gauer, Anniken Helene Aalerud and Nellie Sofie Body
Reviewed by:	Katrine Mo

Avalanche observations versus numerical avalanche model: Simple test of model performance

Contents

Review and reference page

1   Introduction

Hazard assessment for landuse planning in snow avalanche prone areas requires, besides knowledge of return periods, the specification of expected runout distances. For a complete risk assessment, additionally, the intensity of the event, often expressed in terms of impact pressures, and the corresponding vulnerability of endangered objects are needed.

To obtain dynamical parameters, such as velocity, it has become state of practice to use 2-dimensional depth integrated avalanche models like RAMMS (Christen et al. 2010) or SAMOS-AT (Sampl and Granig, 2009). However, those models still lack a thorough and documented validation - which is partly caused by the lack of sufficient avalanche data - and therefore, it requires extensive experience from practitioners to assess the model results. Mainly, the models are calibrated based on runout observation, however runout observations provide limited constraints for the validation of the empirical parameters used in common present-day numerical avalanche models.

On the other hand side, observations of runout distances combined with velocity measurements suggest that "major" dry-mixed avalanches show a scale invariance to the total drop height H_{SC}. This is in accordance to the proposed upper-limit envelope of the maximum velocity by McClung and Schaerer (2003) and a simple scaling analysis using a simple mass block model on cycloidal and parabolic tracks (Gauer, 2018). Therefore, those combined observations give a much more stringent constrain for the parameter choice.

2   Research goals

This note is a continuation of work started in the previous report-period (Issler et al. 2020) and includes a more systematically scanning of the model behavior of two models used in Norway for avalanche simulations.

As mentioned above, the combination of runout observations and velocity scaling can provide a more stringent constraint to the choice of the empirical model parameters for the commonly used friction laws. Choosing a simple track geometry and the use of expected runout and maximum velocities along the track can therefore give a fast impression of model performance versus observations depending on the model parameters.

The approach is exemplified in (Gauer, 2018 and 2020). Figure 1, Figure 2, and Figure 3 show results obtained with a simple mass block model that accounts for mass entrainment. Although only a first order approximation, the model captures the observations for "major" dry-mixed avalanches reasonably well. Therefore, the figures give a reference for the 2D simulations shown in Section 4. As the model is basically scale invariant regarding the drop height H_{SC}, Figure 1 will be similar for various drop heights.
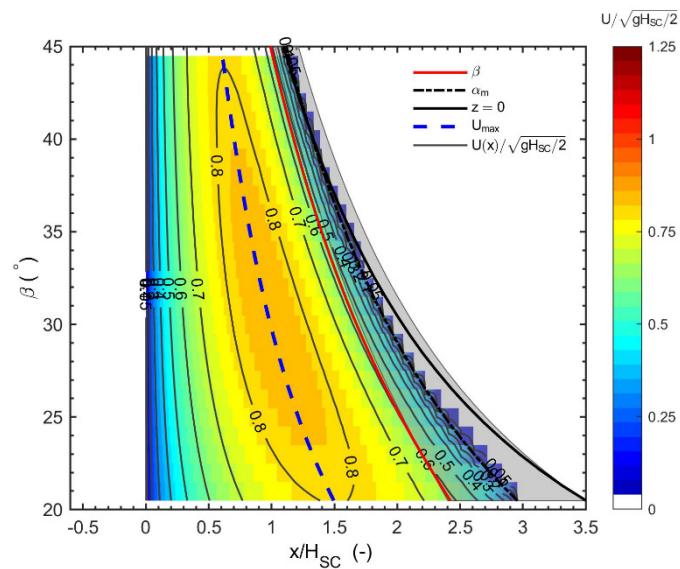
Figure 1 MBVM (Mass Block with Variable Mass): Maximum normalized velocity,
$$\mathbf{U}_m \equiv U \big/ \sqrt{gH_{SC}/2}$$
; iso-lines of scaled avalanche velocities on some parabolic orbits with different steepness given as ϕ_0-angle. Outlet length given to hit the average outlet angle α_m corresponding to the α-β model (Lied and Bakkehøi, 1980). Also marked are corresponding positions of β-, α_m, and where z becomes zero. Gray shaded area shows $\alpha_m \pm \sigma$ range.
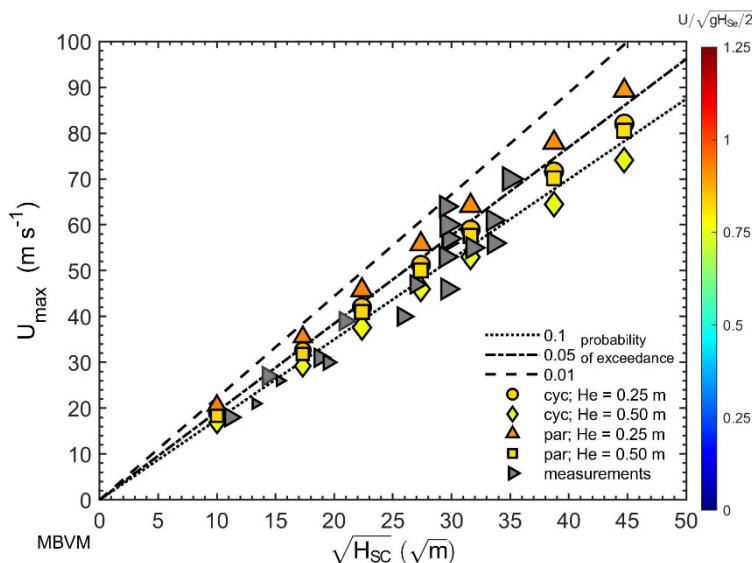

Figure 2 Simulated maximum velocity, U_{max}, versus square root of the drop height, $\sqrt{H_{SC}}$. The color illustrates the scaled velocity $U_{SC} = U_{max} / \sqrt{gH_{SC}/2}$. The figure shows example calculations for a cycloidal and parabolic track and two erosion depths. The initial slope angle ϕ_0 of the tracks is 40°. The gray triangles depict measured maximum front-velocities from major avalanche events in various tracks. The lines depict the probability of exceedance.
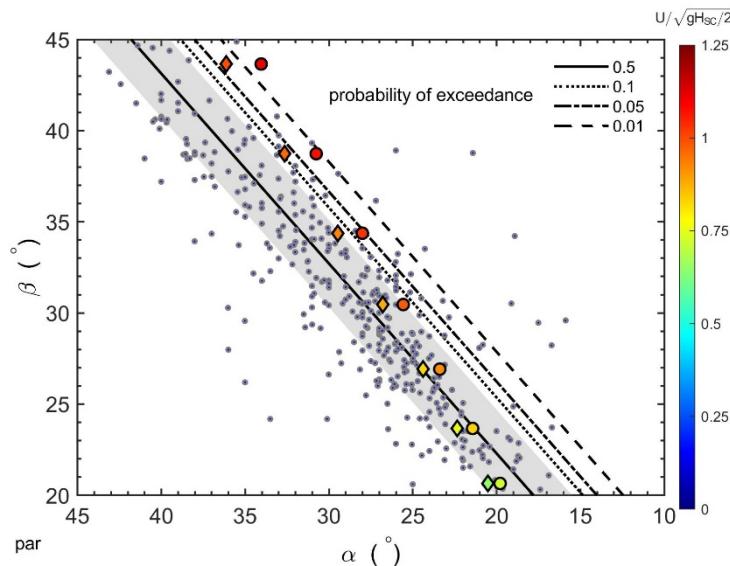
Figure 3 Simulated runout marked by the α-angle and maximum velocity (color coded) on a parabolic track with the mean slope angle, β, as parameter. (•) marks runs with entrainment height He = 0.25 m and (♦) those with He = 0.5 m. Observations are shown as gray dots. Estimated exceedance probabilities of α versus β, according to the α-β model $\alpha_m = 0.96\beta - 1.4°$ (Lied and Bakkehøi, 1980); gray shaded area $\pm\sigma$.

3   Methods

As mentioned, avalanche velocity is an important parameter to characterize the dynamic behavior. Observations imply that the maximum velocity of major avalanches scale with the total drop height HSC, that is $U_{max} \sim \sqrt{gH_{sc}/2}$ (McClung and Gauer, 2018; Gauer, 2018; Gauer, 2014). Combined with estimates on the expected runout of major avalanches, e.g., by using statistical models, these observations provide implications for the choice of the empirical parameters of the Voellmy-model, which is used in most of present-day avalanche models.

Using a simple parabolic track, model performance can be tested. To this end, simulations were performed on slightly channelized parabolic tracks where the thalweg is given by

$$z_1 / H_{SC} = a(x / H_{SC})^2 + b(x / H_{SC}) + c \qquad (1)$$

and

$$z(x,y) = z_1(1 + f(y)) \qquad (2)$$

Here, f(y) defines the degree of canalization. Using a slight canalization should reduce lateral spreading, which is caused by numerical diffusion and therefore is an artefact. The parameters a, b, and c are determined by the initial slope angle ϕ_0 and a proxy of the mean slope angle is $\beta \approx 0.72\phi_0 - 1.4°$ (for explanations see Gauer, 2018), shows an example grid.

At the low point, the track is horizontally extended. The volume is adjusted according to expected deposition volumes (e.g. see Figure 5). The corresponding release areas are located above the actual track (i.e. $z_{SC} > 1$) with an assumed snow height HS = 1, 1.5, and 2 m and a constant slope angle ϕ_0 given by the initial tangent of the track.
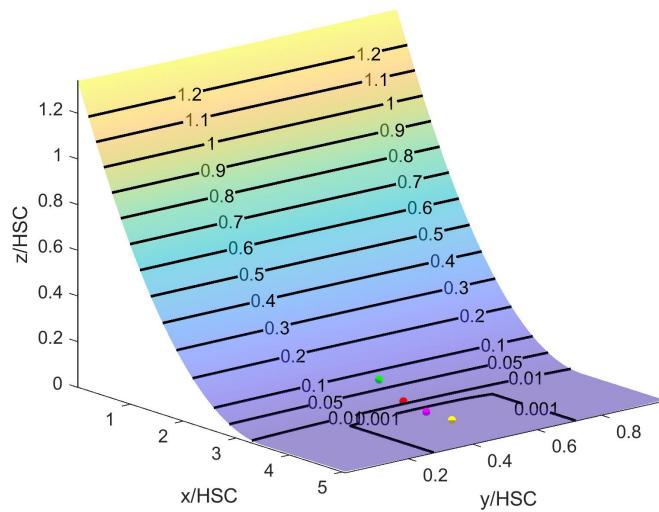

Figure 4 Model grid; the (●) mark the β- and α_m-, (α_m-σ)-, and (α_m-2σ)- points.

The friction parameters are chosen according to standard values for RAMMS corresponding to the respective volume class (Bartelt et al 2017). However, only the highest elevation class is used, which gives the lowest friction values–that is, they should favor longer runouts and higher velocities. Correspondingly *k = g/ξ is chosen for the MoT-Voellmy model.* An overview of the initial and input parameters is summarized in Table 1.

Here we use RAMMS (Christen et al., 2010) using the commercial version 1.7.20 and the build version MoT-Voellmy.2020-05-12.exe. All tests are run without erosion.

NGI
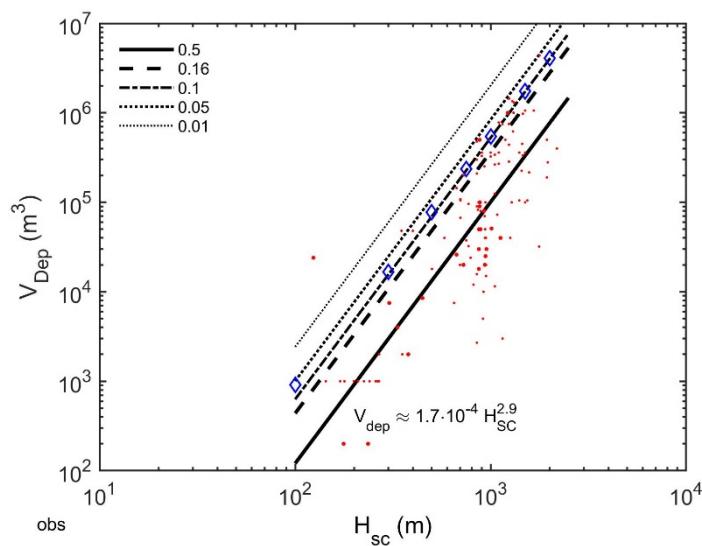
Figure 5 Observed avalanche deposits of "major events" versus total drop height H_{SC} (for references to the data see Gauer et al. 2010). (◊) indicate some of the volumes used in the model simulations in the next section. The lines show the estimated exceedance probabilities derived from these observations.

Table 1 Overview of the various input and terrain parameters used in the simulations.

Initial slope ϕ_0 (°)	Snow height HS (m)	Drop height H_{SC} (m)	Fracture depth D (m)	Volume (m³)	Turbulent drag MoT k (m)	Dry-friction μ (-)	Turbulent drag RAMMS ξ (m s⁻²)
40	1	100	0.8	699	0.00654	0.275	1500
		300		12 258	0.004905	0.235	2000
		500		49 754	0.003924	0.195	2500
		750		161 461	0.00327	0.155	3000
		1000		366 154	0.00327	0.155	3000
		1500		1 170 947	0.00327	0.155	3000
		2000		2 712 440	0.00327	0.155	3000
	1.5	100	1.1	1 049	0.00654	0.275	1500
		300		18 387	0.004905	0.235	2000
		500		74 630	0.00327	0.155	3000
		750		242 191	0.00327	0.155	3000
		1000		549 231	0.00327	0.155	3000
		1500		1 756 421	0.00327	0.155	3000
		2000		4 068 660	0.00327	0.155	3000
	2	100	1.5	1 399	0.00654	0.275	1500
		300		24 516	0.004905	0.235	2000
		500		99 507	0.00327	0.155	3000
		750		322 921	0.00327	0.155	3000
		1000		732 307	0.00327	0.155	3000

Initial slope ϕ_0 (°)	Snow height HS (m)	Drop height H_{SC} (m)	Fracture depth D (m)	Volume (m³)	Turbulent drag MoT k (m)	Dry-friction μ (-)	Turbulent drag RAMMS ξ (m s^{-2})
		1500		2 341 895	0.00327	0.155	3000
		2000		5 424 880	0.00327	0.155	3000
45	1	100	0.7	675	0.00654	0.275	1500
		300		11 383	0.004905	0.235	2000
		500		50 686	0.003924	0.195	2500
		750		159 822	0.00327	0.155	3000
		1000		365 992	0.00327	0.155	3000
		1500		1 172 692	0.00327	0.155	3000
		2000		2 714 634	0.00327	0.155	3000
	1.5	100	1.1	1 012	0.00654	0.275	1500
		300		17 066	0.004905	0.235	2000
		500		75 277	0.00327	0.155	3000
		750		239 620	0.00327	0.155	3000
		1000		548 729	0.00327	0.155	3000
		1500		1 758 209	0.00327	0.155	3000
		2000		4 070 030	0.00327	0.155	3000
	2	100	1.4	1 350	0.00654	0.275	1500
		300		22 766	0.004905	0.235	2000
		500		101 373	0.00327	0.155	3000
		750		319 644	0.00327	0.155	3000
		1000		731 984	0.00327	0.155	3000
		1500		2 345 385	0.00327	0.155	3000
		2000		5 429 267	0.00327	0.155	3000
30	1	100	0.9	700	0.00654	0.275	1500
		300		11 558	0.004905	0.235	2000
		500		50 289	0.003924	0.195	2500
		750		160 475	0.00327	0.155	3000
		1000		366 356	0.00327	0.155	3000
		1500		1 177 402	0.00327	0.155	3000
		2000		2 720 837	0.00327	0.155	3000
	1.5	100	1.3	1 050	0.00654	0.275	1500
		300		17 337	0.004905	0.235	2000
		500		75 433	0.00327	0.155	3000
		750		240 713	0.00327	0.155	3000
		1000		549 534	0.00327	0.155	3000
		1500		1 766 102	0.00327	0.155	3000
		2000		4 081 256	0.00327	0.155	3000
	2	100	1.7	1 400	0.00654	0.275	1500
		300		23 115	0.004905	0.235	2000
		500		100 578	0.00327	0.155	3000
		750		320 951	0.00327	0.155	3000

Initial slope ϕ_0 (°)	Snow height HS (m)	Drop height H_{SC} (m)	Fracture depth D (m)	Volume (m³)	Turbulent drag MoT k (m)	Dry-friction μ (-)	Turbulent drag RAMMS ξ (m s⁻²)
		1000		732 712	0.00327	0.155	3000
		1500		2 354 803	0.00327	0.155	3000
		2000		5 441 675	0.00327	0.155	3000
35	1	100	0.8	700	0.00654	0.275	1500
		300		11 556	0.004905	0.235	2000
		500		50 064	0.003924	0.195	2500
		750		159 536	0.00327	0.155	3000
		1000		368 939	0.00327	0.155	3000
		1500		1 172 392	0.00327	0.155	3000
		2000		2 719 856	0.00327	0.155	3000
	1.5	100	1.2	1 049	0.00654	0.275	1500
		300		16 389	0.004905	0.235	2000
		500		75 066	0.00327	0.155	3000
		750		239 206	0.00327	0.155	3000
		1000		553 183	0.00327	0.155	3000
		1500		1 757 873	0.00327	0.155	3000
		2000		4 078 124	0.00327	0.155	3000
	2	100	1.6	1 399	0.00654	0.275	1500
		300		23 111	0.004905	0.235	2000
		500		100 128	0.00327	0.155	3000
		750		319 072	0.00327	0.155	3000
		1000		737 878	0.00327	0.155	3000
		1500		2 344 784	0.00327	0.155	3000
		2000		5 439 713	0.00327	0.155	3000
50	1	100	0.6	674	0.00654	0.275	1500
		300		11 100	0.004905	0.235	2000
		500		51 362	0.003924	0.195	2500
		750		162 238	0.00327	0.155	3000
		1000		367 709	0.00327	0.155	3000
		1500		1 172 680	0.00327	0.155	3000
		2000		2 710 621	0.00327	0.155	3000
	1.5	100	1.0	1 012	0.00654	0.275	1500
		300		16 667	0.004905	0.235	2000
		500		77 123	0.00327	0.155	3000
		750		243 610	0.00327	0.155	3000
		1000		549 846	0.00327	0.155	3000
		1500		1 760 847	0.00327	0.155	3000
		2000		4 082 873	0.00327	0.155	3000
	2	100	1.3	1 349	0.00654	0.275	1500
		300		22 217	0.004905	0.235	2000
		500		102 805	0.00327	0.155	3000

Initial slope ϕ_0 (°)	Snow height HS (m)	Drop height H_{SC} (m)	Fracture depth D (m)	Volume (m³)	Turbulent drag MoT k (m)	Dry-friction μ (-)	Turbulent drag RAMMS ξ (m s⁻²)
		750		324 729	0.00327	0.155	3000
		1000		735 992	0.00327	0.155	3000
		1500		2 347 187	0.00327	0.155	3000
		2000		5 442 419	0.00327	0.155	3000
55	1	100	0.6	674	0.00654	0.275	1500
		300		11 697	0.004905	0.235	2000
		500		49 840	0.003924	0.195	2500
		750		160 351	0.00327	0.155	3000
		1000		366 083	0.00327	0.155	3000
		1500		1 170 434	0.00327	0.155	3000
		2000		2 725 712	0.00327	0.155	3000
	1.5	100	0.9	1 011	0.00654	0.275	1500
		300		17 556	0.004905	0.235	2000
		500		74 804	0.00327	0.155	3000
		750		240 666	0.00327	0.155	3000
		1000		549 444	0.00327	0.155	3000
		1500		1 756 672	0.00327	0.155	3000
		2000		4 090 946	0.00327	0.155	3000
	2	100	1.1	1 348	0.00654	0.275	1500
		300		23 414	0.004905	0.235	2000
		500		99 767	0.00327	0.155	3000
		750		320 981	0.00327	0.155	3000
		1000		732 805	0.00327	0.155	3000
		1500		2 342 910	0.00327	0.155	3000
		2000		5 456 180	0.00327	0.155	3000

4 Results

Figure 6 and Figure 7 show plots corresponding to Figure 1. The values in both cases are taken along the center line of the track. On a first glance, the results suggest that the models are capable to capture the runout distances reasonably well, although one could have expected even longer runouts with respect to the model setting, see also Figure 10. There are, however, noticeable difference between the predicted maximum velocities and those observed, especially for avalanche drops heights larger 1000 m. This is also very well reflected in Figure 11. But also, for smaller drop heights it seems there are differences in the velocity profiles and that the simulations reach its maximum velocity early on and underestimate the velocity the lower part of the track. RAMMS and MoT-Voellmy show quite similar behaviour.

NGI
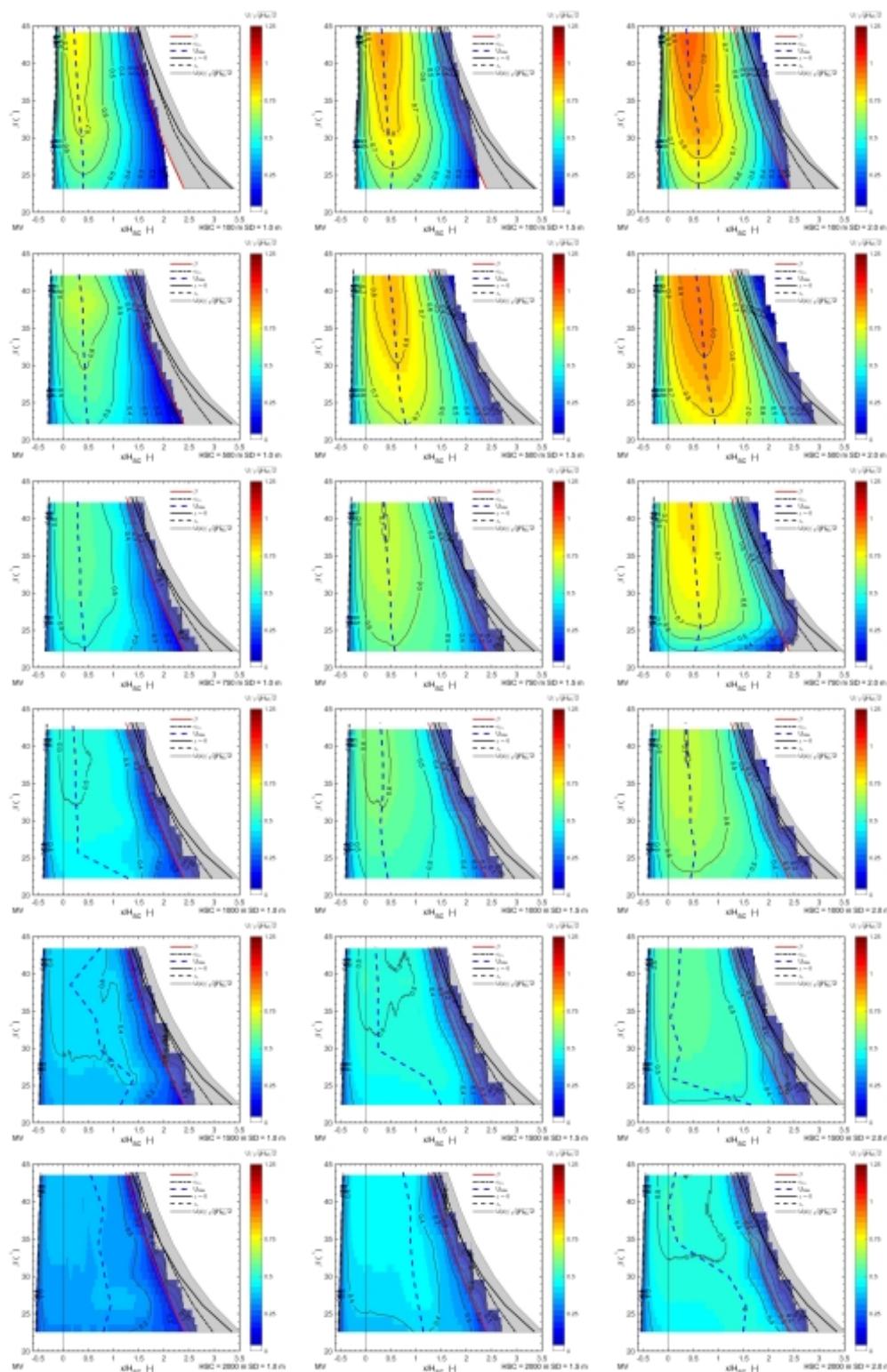
Figure 6 MoT-Voellmy: Maximum normalized velocity, $\mathbf{U}_m \equiv U / \sqrt{gH_{SC}/2}$ *, along the center line*
for various drop heights, H_{SC} = [100, 500, 750, 1000, 1500, 2000] m (top to bottom) and snow
*height, HS = [1 ,1.5, 2] m (left to right).*
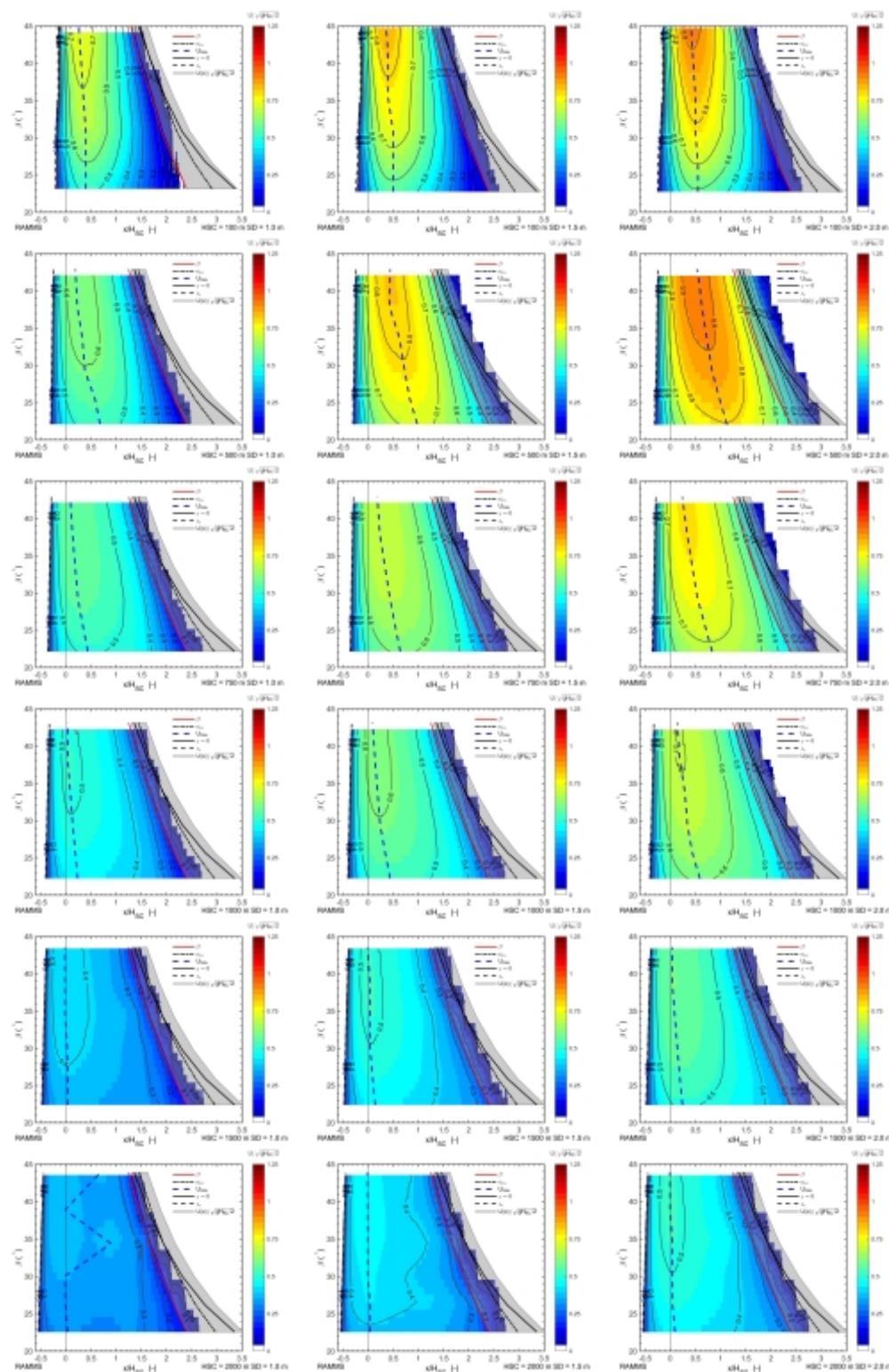
Figure 7 RAMMS: Maximum normalized velocity, $\mathbf{U}_m \equiv U\big/\sqrt{gH_{SC}/2}$ *, along the center line for various drop heights, H_{SC} = [100, 500, 750, 1000, 1500, 2000] m (top to bottom) and snow depth, HS = [1 ,1.5, 2] m (left to right).*
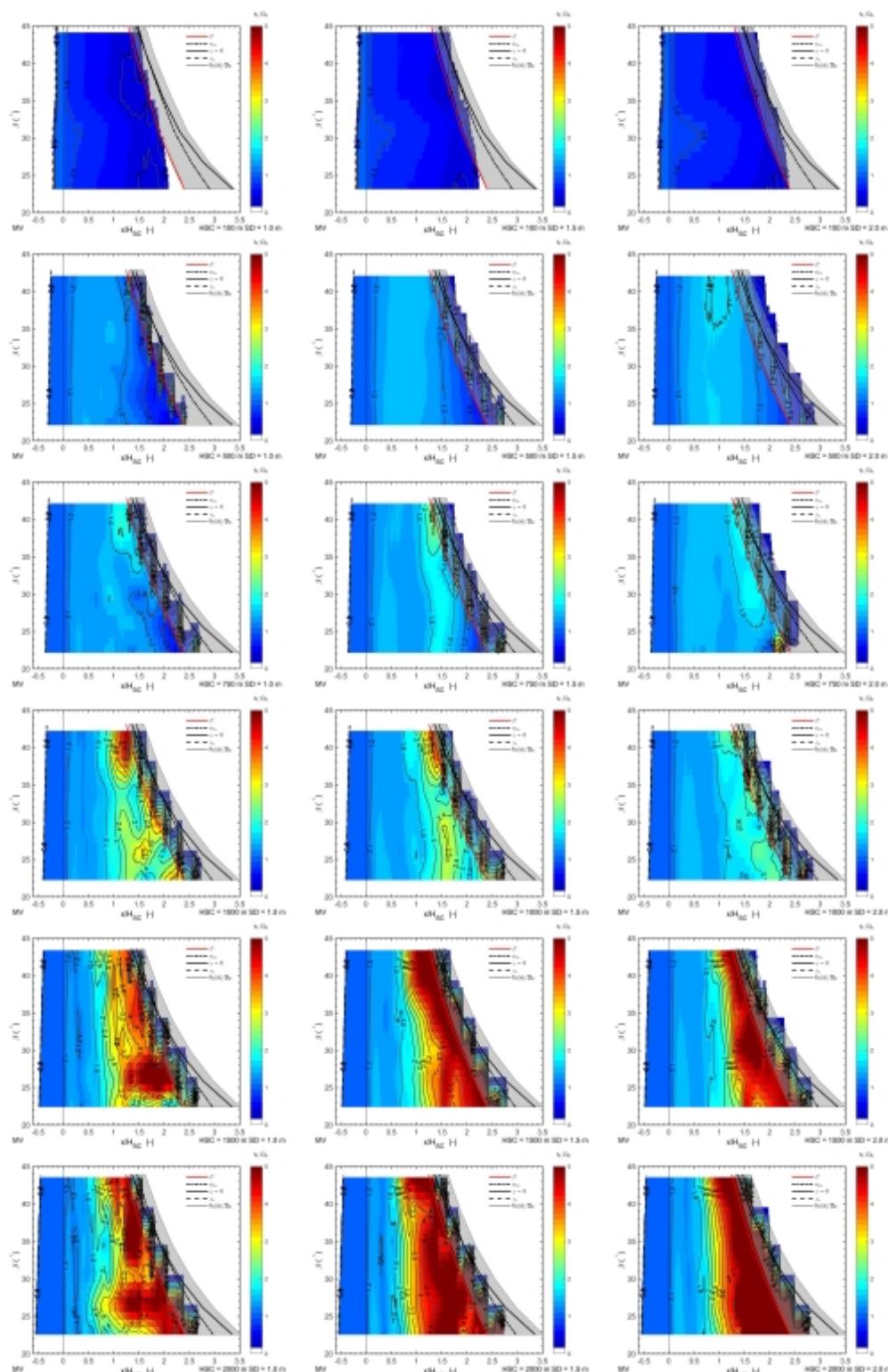
Figure 8 MoT-Voellmy: Maximum relative flow depth h_f/HS along the center line for various drop heights, H_{SC} = [100, 500, 750, 1000, 1500, 2000] m (top to bottom) and snow depth, HS = [1 ,1.5, 2] m (left to right).
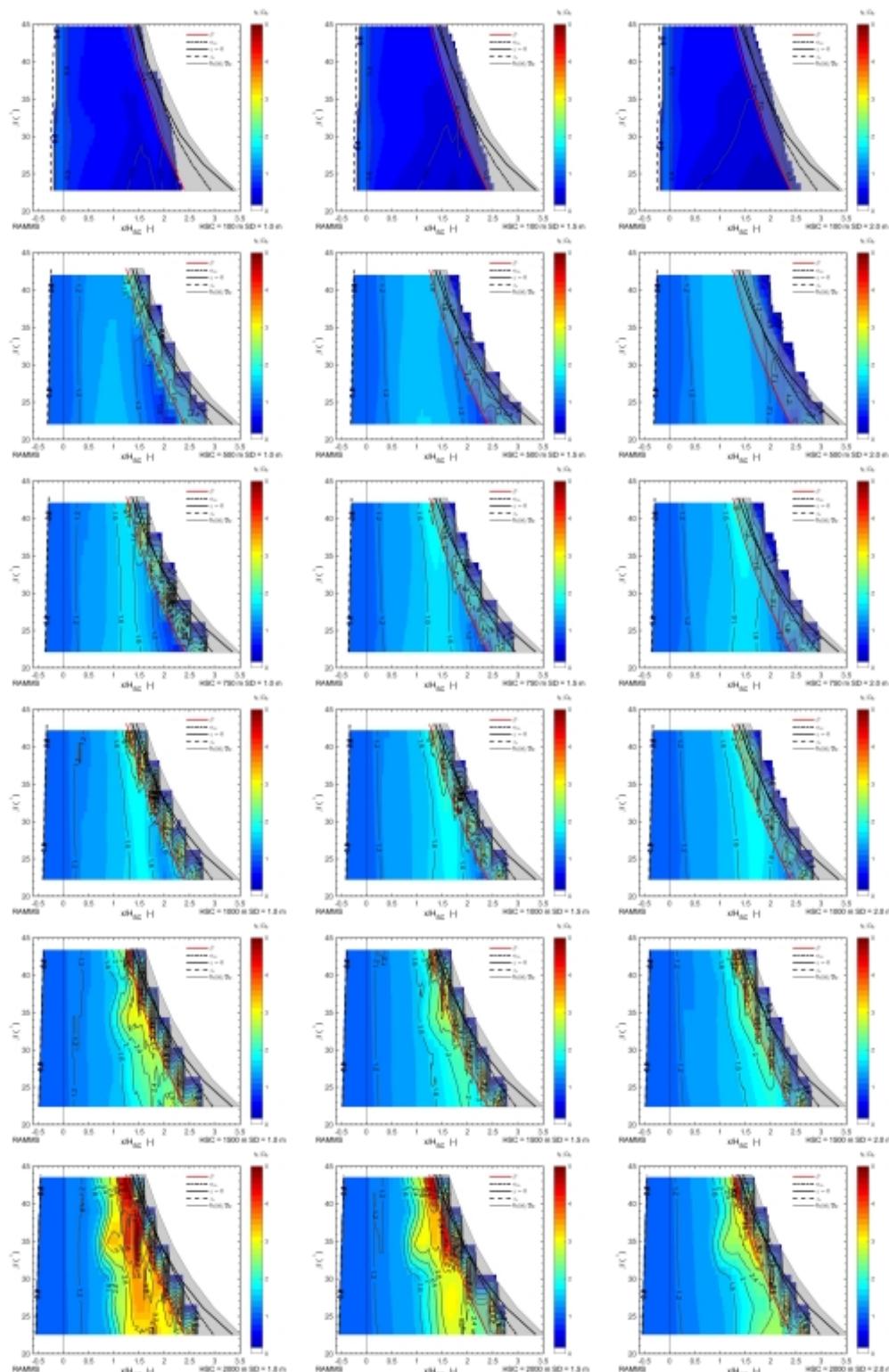
Figure 9 RAMMS: Maximum relative flow depth h_f/HS along the center line for various drop heights, H_{SC} = [100, 500, 750, 1000, 1500, 2000] m (top to bottom) and snow depth, HS = [1 ,1.5, 2] m (left to right).

Figure 8 and Figure 9 show the simulated maximum flow depth scaled by the initial fractur depth. Here, little systematic observations are available, hence a comparison with observation is not possible. However, it can be noticed that here are considerable differences in between the models RAMMS and MoT-Voellmy. Some of those values seem to be influenced be the numeric.

Figure 10 gives a summary of the simulated runout angles. As mentioned the model seem to capture the expected runout according to the observations. However, one could have expected longer runouts considering the simulation setup that should have favoured higher velocities and longer runout. Also, it can be noticed that there is a slight increase in runout length with increasing slope steepness.
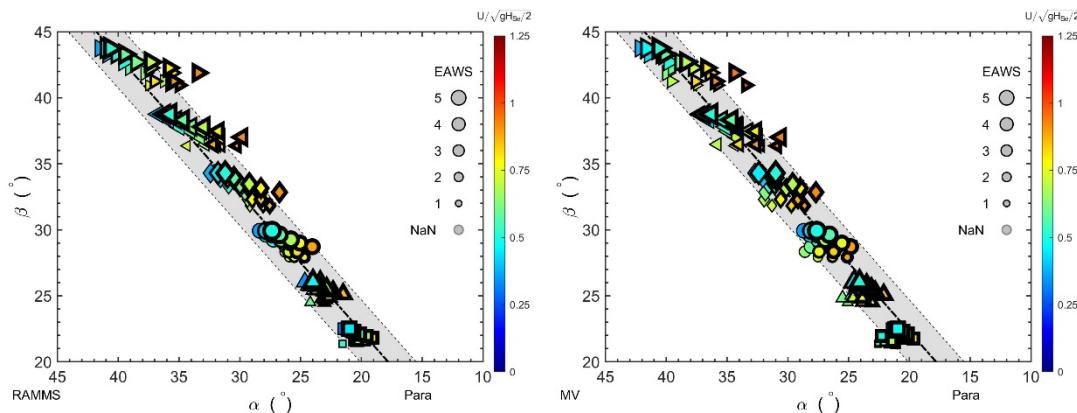
Figure 10 Simulated runout marked by the α-angle and maximum velocity (color coded) on a parabolic track with the mean slope angle, β (varying symbol) and snow depth HS (varying symbol outline) as parameter. Expected runout angle α versus β, according to the α-β model $\alpha_m = 0.96\beta - 1.4°$ (Lied and Bakkehøi, 1980); gray shaded area $\pm\sigma$. Simple size gives an impression of the avalanche size according to EAWS volume classification. On the left: RAMMS; on the right MoT-Voellmy.
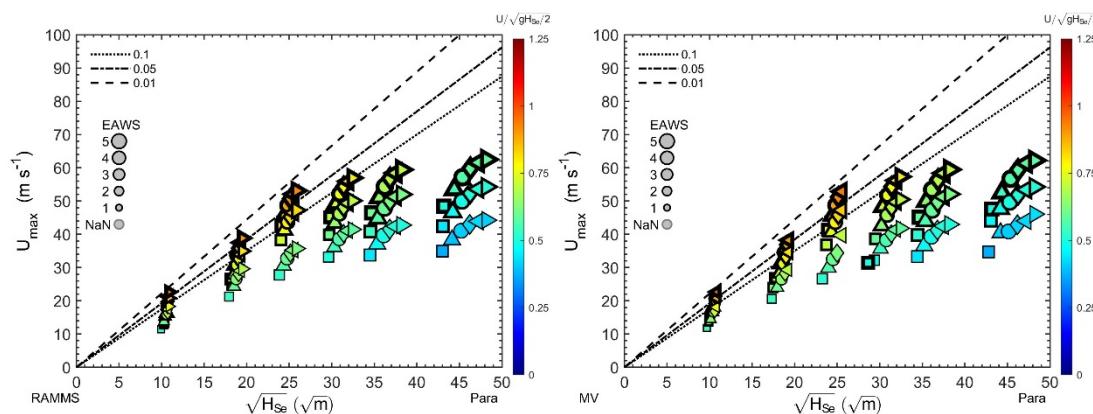
Figure 11 Simulated maximum velocity, U_{max}, versus square root of the drop height, $\sqrt{H_{SC}}$ with the mean slope angle, β (varying symbol for comparison see Figure 10) and snow depth HS = [1, 1.5, 2] m (varying symbol outline) as parameter. The color illustrates the scaled velocity $U_{SC} = U_{max} / \sqrt{gH_{SC}/2}$.

For many practitioners an important question is the velocity at a beginning of the runout area regarding the design of mitigation measures, such as catching- or deflection-dams. Figure 12 shows a comparison of simulated maximum velocity at the β-point for the mass block (MB), Mot-Voellmy (MV) and RAMMS. As earlier mentioned, Mot-Voellmy and RAMMS behave quite similar, however there is are considerable differences in respect to the mass block model. This suggests that the two models underestimate the velocity, most pronounced for shallow slopes. Considering that the velocity is a major design criterion, the deficiency is crucial.
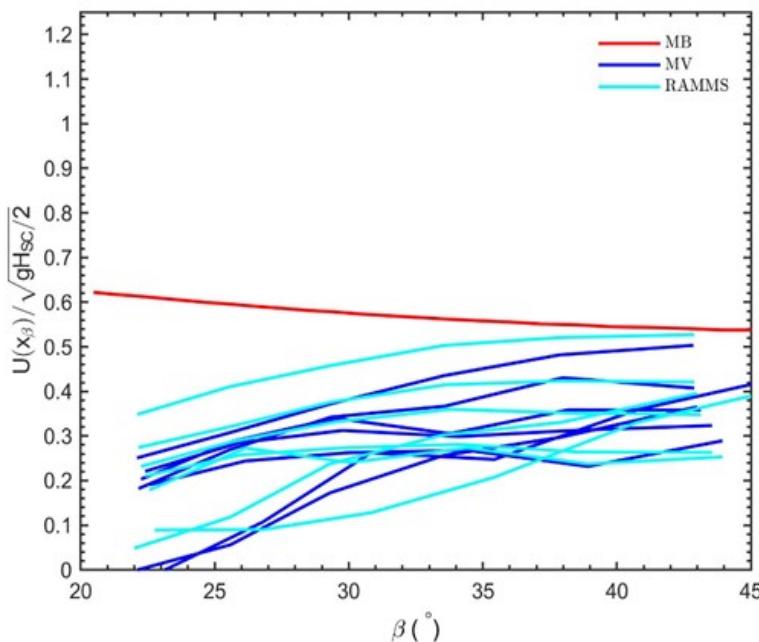
Figure 12 Normalized velocity $\mathbf{U} = U(x_\beta)\big/\sqrt{gH_{SC}/2}$ at the β-point for various β-angles and different drop-heights.

The presented simulations reveal again some of the known deficiencies of the Voellmy-friction law and its commonly proposed parameter set in respect to major dry mixed avalanches.

Gauer and Issler (2004) and Sovilla (2004) emphasized the importance of mass entrainment long the avalanche track. Gauer and Issler noted that erosion and entrainment of mass can contribute considerably to the retardation of an avalanche. They estimated a ratio between the contribution due to entrainment and due to frictional losses of the order of 0.2. The effect of erosion was recently demonstrated by Gauer (2020) using a simple mass block model. He demonstrated that the model is capable to predict runout distances reasonably well while also reproduce the observed velocity scaling:

NGI

$$\mathbf{U}_m \equiv \frac{U}{\sqrt{gH_{SC}}} = \sqrt{\frac{\left(\sin\phi_m - a_0\cos\phi_m - \dfrac{K_e\sqrt{2d_e}}{gH_{SC}\,m(\varsigma_m)}\right)}{a_0 c(\varsigma_m, \phi_0) + \dfrac{\rho_s d_e}{m(\varsigma_m)}}} \tag{3}$$

$$\mathbf{U}_m \approx \frac{1}{\sqrt{2}}$$

where

- U is the velocity (m s^{-1})
- H_{SC} is the total drop height (m)
- g is the gravitational acceleration (m s^{-2})
- ϕ_m is the slope angle at the location of the maximum (°)
- a_0 is the apparent friction factor (-)
- K_e fracture toughness (kPa $\sqrt{m}$)
- d_e erosion depth (m)
- ρ_s density of the snowpack (kg m^{-3})
- $c(\zeta_m, \phi_0)$ curvature factor (-)
- $m(\zeta_m)$ scaled avalanche mass M/(H_{SC} w) (kg m)
- w is the avalanche width (m)
- ζ_m scaled length, s/H_{SC} along the track (-)
- $()_m$ subscript m marks the location of the maximum velocity

Eq. (3) reveals the influence and importance of the erosion term $\rho_s d_e / m(\varsigma)$. Firstly, this contribution to the retardation of the avalanche is not constant along the track—with increasing mass its contribution decreases. Furthermore, high avalanche velocities and longer runouts are favoured by a small ratio $\rho_s d_e / m(\varsigma)$. This suggest that the relative magnitude of the release mass m(ζ_0) = M$_0$/(H_{SC} w) is of major importance for large size avalanches, here is the width of the release area.

At the same time Eq. (4) gives some indications how to adapted the friction parameter for the Voellmy-models to better reproduce the observed velocities along the track for major dry-mixed avalanches. The simulation the mass block model suggests

$$a_0 \approx 0.3 \tag{5}$$

Observations of velocities and outlet distances for rare dry avalanches suggest the order of magnitude relationship (Gauer, 2014):

$$\overline{a_2} H_{SC} = O(0.1) \tag{6}$$

where $\overline{a_2}$ gives an average value. Comparing Eq. (3) with a PCM-type model results in an initial estimate for the order of a$_2$:

$$a_2(s) \approx \frac{\rho_s(s)d_e(s)w(s)}{M_a(s)} \tag{7}$$

where $M_a(s)$ is the avalanche mass at position s along the track and w is the avalanche width. The relationship between PCM-type model and Voellmy-type model give $a_2 \equiv g/\xi h_1$, where h_1 is the flow height. Therefore, it might be possible to a certain degree to adapt μ and ξ used in RAMMS. However, whereas the ξ is more or less a constant in RAMMS, the square dependent term due to erosion varies along the track as the total mass varies along the track as the total mass varies. If one disregards mass loss due to deposition and assumes a constant width w of the track, Eq. (7) can be rewritten for a cycloidal track as

$$\frac{gH_{SC}}{\xi(\zeta)h_f(\zeta)} = \chi \sin\phi_0 \frac{1}{\left(1 + 2\chi \frac{(\sin\phi_0 - \sin\phi_1(\zeta))}{\sin\phi_0}\right)} \tag{8}$$

where

$$\chi = \frac{\rho_s H_e}{c_0 \; \rho_r HS} \frac{\cos(\phi(\zeta))}{\cos(\phi_0)}$$

c_0 is a coefficient describing the length of the release area and is expected to be in the range of 0.1 to 0.3 for major avalanches.

Small values of χ favor higher velocities and longer runout distances.

5   Concluding Remarks

In this note, a simple track geometry was used to test the performance of present days avalanche models. The model tracks varied in drop height and mean steepness. The model results were compared with expected values of the maximum velocity and runout based on avalanche observations.

On a first glance, the results suggest that RAMMS and MoT-Voellmy are capable to capture the statistical mean runout distances reasonably well, although one could have expected even longer runouts with respect to the model setting. There are, however, noticeable difference between the predicted maximum velocities and those observed, especially for avalanche drops heights larger 1000 m. Also, for smaller drop heights, it seems there are differences in the velocity profiles and that the simulation reaches its maximum velocity early on and underestimate the velocity the lower part of the track.

It might be possible to adapt the model parameters to a certain degree to compensate for the short comings, however, as long as the parameters are static and erosion is not directly included, this is only regarded as a patch for the models.

Here, we focused mainly on RAMMS and on MOT-Voellmy, but similar results are expected and are known for other models using the Voellmy-rheology too, like DAN3D (Aron et al. 2016; Conlan, et al. 2018) or SAMOS-AT (Sample and Granig, 2009).

6   References

Bartelt, P., Bühler, Y., Christen, M., Deubelbeiss, Y., Salz, M., Schneider, M., and Schumacher, L. (2017). RAMMS User Manual v.1.7.0 Avalanche. WSL Institute for Snow and Avalanche Research SLF.

Aaron, J., Conlan, M., Johnston, K., Gauthier, D., and McDougall, D. (2016). Adapting and calibrating the dan3d dynamic model for North American snow avalanche runout modelling. In International Snow Science Workshop 2016 Proceedings, Breckenridge, CO, USA.

Christen, M.; Kowalski, J. & Bartelt, P. (2010) RAMMS: Numerical simulation of dense snow avalanches in three-dimensional terrain, Cold Regions Science and Technology, 2010, 63, 1-14

Conlan, M., Aaron, J., Johnston, K., Gauthier, D., and McDougall, S. (2018). Dan3D model parameters for snow avalanche case studies in Western Canada. In Dan3D Model Parameters for Snow Avalanche Case Studies in Western Canada, pages 783–787.

Gauer, P., Issler, D., 2004. Possible erosion mechanisms in snow avalanches. Ann. Glaciol. 38, 384–392. https://doi.org/10.3189/172756404781815068.

Gauer, P.; Kronholm, K.; Lied, K.; Kristensen, K. & Bakkehøi, S. (2010) Can we learn more from the data underlying the statistical α-β model with respect to the dynamical behavior of avalanches? Cold Regions Science and Technology, 2010, 62, 42-54

Gauer, P. (2014) Comparison of avalanche front velocity measurements and implications for avalanche models, Cold Regions Science and Technology, 2014, 97, 132-150

Gauer, P. (2018) Considerations on scaling behavior in avalanche flow along cycloidal and parabolic tracks, Cold Regions Science and Technology, 2018, 151, 34-46

Gauer, P. (2020) Considerations on scaling behavior in avalanche flow: Implementation in a simple mass block model, Cold Regions Science and Technology, 2020, 180, 103165

Issler, D.; Gauer, P.; Glimsdal, S.; Jaedicke, C.; Sandersen, F and Gisnås, K. G. SP4 FoU Snøskred-ANNUAL REPORT 2019 Norwegian Geotechnical Institute, Norwegian Geotechnical Institute, 2020

Lied, K., Bakkehøi, S., 1980. Empirical calculations of snow-avalanche run-out distance based on topographic parameters. J. Glaciol. 26, 165–177.

McClung, D. M. and Gauer, P. (2018) Maximum frontal speeds, alpha angles and deposit volumes of flowing snow avalanches, Cold Regions Science and Technology, 2018, 153, 78-85

McClung, D. & Schaerer, P. (2006) The Avalanche Handbook, The Mountaineers Books, 2006

Sampl, P. & Granig, M. (2009) Avalanche Simulation with SAMOS-AT Proceedings of the International Snow Science Workshop, Davos, 2009, 519-523

Sovilla, B., 2004. Field experiments and numerical modelling of mass entrainment and deposition processes in snow avalanches. Diss. ETH no. 15462. ETH Zurich. Zurich, Switzerland. https://doi.org/10.3929/ethz-a-004784844.

Dokumentinformasjon/*Document information*

Dokumenttittel/*Document title*	Dokumentnr./*Document no.*
Avalanche observations versus numerical avalanche model: Simple test of model performance	20200017-04-TN

Dokumenttype/*Type of document*	Oppdragsgiver/*Client*	Dato/*Date*
Teknisk notat / Technical note	NVE	2021-03-22

Rettigheter til dokumentet iht kontrakt/ *Proprietary rights to the document according to contract*	Rev.nr.&dato/*Rev.no.&date*
Oppdragsgiver / Client	0 /

Distribusjon/*Distribution*
ÅPEN: Skal tilgjengeliggjøres i åpent arkiv (BRAGE) / OPEN: To be published in open archives (BRAGE)

Emneord/*Keywords*
Norwegian_avalanche_grant

Stedfesting/*Geographical information*

Land, fylke/*Country*	Havområde/*Offshore area*
Norway	
Kommune/*Municipality*	**Feltnavn/*Field name***
Stryn	
Sted/*Location*	**Sted/*Location***
Grasdalen	
Kartblad/*Map*	**Felt, blokknr./*Field, Block No.***
UTM-koordinater/*UTM-coordinates* Zone: East: North:	**Koordinater/*Coordinates*** Projection, datum: East: North:

Dokumentkontroll/*Document control*
Kvalitetssikring i henhold til/*Quality assurance according to NS-EN ISO9001*

Rev/ *Rev.*	Revisjonsgrunnlag/*Reason for revision*	Egenkontroll av/ *Self review by:*	Sidemanns-kontroll av/ *Colleague review by:*	Uavhengig kontroll av/ *Independent review by:*	Tverrfaglig kontroll av/ *Interdisciplinary review by:*
0	Original document	2021-03-19 Peter Gauer	2021-03-19 Katrine Mo		

Dokument godkjent for utsendelse/ *Document approved for release*	Dato/*Date*	Prosjektleder/*Project Manager*
	19 March 2021	Christian Jaedicke

2015-10-16, 043 n/e, rev.03

\\xfil1\ProData$\2020\00\20200017\WP0 - Project Admin\Delivery-Result\Technical-notes\20200017-04-TN_CompObsModel\20200017-04-TN_CompObsModel_final.docx

NGI
OSLO
TRONDHEIM
HOUSTON
PERTH